



Cite this: *Chem. Sci.*, 2024, **15**, 757

All publication charges for this article have been paid for by the Royal Society of Chemistry

## Selective FRET nano probe based on carbon dots and naphthalimide–isatin for the ratiometric detection of peroxynitrite in drug-induced liver injury†

Yueci Wu, <sup>‡a</sup> Lu-Lu Sun, <sup>‡cd</sup> Hai-Hao Han, <sup>\*cd</sup> Xiao-Peng He, <sup>\*ef</sup> Weiguo Cao <sup>\*b</sup> and Tony D. James <sup>\*ag</sup>

Drug-induced liver injury (DILI) is the most common cause for acute liver failure in the USA and Europe. However, most of DILI cases can recover or be prevented if treatment by the offending drug is discontinued. Recent research indicates that peroxynitrite ( $\text{ONOO}^-$ ) can be a potential indicator to diagnose DILI at an early stage. Therefore, the establishment of an assay to detect and track  $\text{ONOO}^-$  in DILI cases is urgently needed. Here, a FRET-based ratiometric nano fluorescent probe CD-N-I was developed to detect  $\text{ONOO}^-$  with high selectivity and excellent sensitivity. This probe consists of carbon dots and a naphthalimide–isatin peroxynitrite sensing system assembled based on electrostatic interactions. Using CD-N-I we were able to detect exogenous  $\text{ONOO}^-$  in live cells and endogenous  $\text{ONOO}^-$  in APAP-induced liver injury of HepG2 cells.

Received 23rd September 2023  
Accepted 22nd November 2023

DOI: 10.1039/d3sc05010f  
[rsc.li/chemical-science](http://rsc.li/chemical-science)

## Introduction

As a vital organ in the human body, the liver has multiple biological functions, including the immune response and vitamin storage.<sup>1</sup> One of its key roles is to remove drugs from the body. This makes the liver a main target for drug-induced damage.<sup>2</sup> Adverse drug reactions and overdoses are the main causes of drug-induced liver injury (DILI).<sup>3,4</sup> Acetaminophen (APAP), as

a typical analgesic and antipyretic drug, has been widely studied since a large number of DILI cases are related to the use of APAP.<sup>5</sup> Recent studies have found that peroxynitrite ( $\text{ONOO}^-$ ) could be formed in vascular lumen during early stages of treatment or due to an overdose of APAP.<sup>4</sup> As an early event in DILI, reactive metabolites of APAP can bind to proteins in hepatocytes, leading to mitochondrial oxidative stress.<sup>4,6</sup> Then, due to mitochondrial dysfunction, the respiratory chain becomes inhibited, and the level of superoxide increases.<sup>2,4,7</sup> When superoxide reacts with nitric oxide,  $\text{ONOO}^-$  is formed and promotes intracellular protein nitration.<sup>4,8–10</sup> Meanwhile, with the continuous generation of intracellular  $\text{ONOO}^-$ , parenchymal injury of hepatocytes is simultaneously aggravated.<sup>4</sup> In addition, immune-mediated injury, as one critical mechanism of DILI, can not only lead to antibody-mediated cell death but also the release of reactive oxygen species (ROS) and cytokines, which results in hepatic injury.<sup>2,11</sup> However, most DILI cases can recover or be prevented from developing into chronic liver disease and acute liver failure if treatment by the offending drug is discontinued.<sup>2,12</sup> At the same time,  $\text{ONOO}^-$ , as a ROS, can provide a potential indicator to diagnose drug-induced liver injury at an early stage. In general, up to 5  $\mu\text{M}$  of  $\text{ONOO}^-$  exhibits a protective role towards the cardiovascular endothelium.<sup>13</sup> However, when RAW 264.7 cells are exposed to 10–100  $\mu\text{M}$  for 14 hours, cell apoptosis is observed.<sup>14,15</sup> So, it is important to establish an assay to detect and track  $\text{ONOO}^-$  selectively, sensitively and rapidly, especially in DILI.

Currently, electrochemical sensors, nitrotyrosine detection and fluorescence monitoring are the most commonly used

<sup>a</sup>Department of Chemistry, University of Bath, Bath, BA2 7AY, UK. E-mail: [t.d.james@bath.ac.uk](mailto:t.d.james@bath.ac.uk)

<sup>b</sup>Department of Chemistry, Shanghai University, Shanghai 200444, P. R. China. E-mail: [wgcao@shu.edu.cn](mailto:wgcao@shu.edu.cn)

<sup>c</sup>Shandong Laboratory of Yantai Drug Discovery, Bohai Rim Advanced Research Institute for Drug Discovery, Yantai, Shandong 264117, P. R. China. E-mail: [hanhaihao@simm.ac.cn](mailto:hanhaihao@simm.ac.cn)

<sup>d</sup>Molecular Imaging Center, Shanghai Institute of Materia Medica, Chinese Academy of Sciences, Shanghai 201203, P. R. China

<sup>e</sup>Key Laboratory for Advanced Materials, Joint International Research Laboratory of Precision Chemistry and Molecular Engineering, Feringa Nobel Prize Scientist Joint Research Center, Frontiers Center for Materiobiology and Dynamic Chemistry, School of Chemistry and Molecular Engineering, East China University of Science and Technology, 130 Meilong Rd, Shanghai 200237, P. R. China. E-mail: [xphe@ecust.edu.cn](mailto:xphe@ecust.edu.cn)

<sup>f</sup>The International Cooperation Laboratory on Signal Transduction, National Center for Liver Cancer, Eastern Hepatobiliary Surgery Hospital, Shanghai 200438, P. R. China

<sup>g</sup>School of Chemistry and Chemical Engineering, Henan Normal University, Xinxiang 453007, P. R. China

† Electronic supplementary information (ESI) available. See DOI: <https://doi.org/10.1039/d3sc05010f>

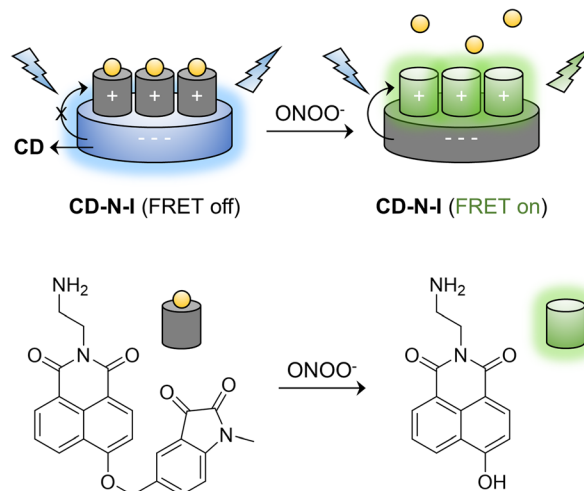
‡ These authors contributed equally.



methods to detect  $\text{ONOO}^-$ .<sup>16,17</sup> Electrochemical sensors detect  $\text{ONOO}^-$  through electrocatalytic reduction.<sup>16,17</sup> However, due to pH dependence of the peak potential and biocompatibility problems caused by implantation, the application of this approach is limited in complicated biological systems.<sup>17-20</sup> The nitrotyrosine assay indirectly measures  $\text{ONOO}^-$  through the measurement of the concentration of nitrotyrosine formed by the nitration of tyrosine, determined using analytical approaches, such as HPLC, LC-MS or GC-MS.<sup>21-24</sup> However, this method is not suitable for detecting  $\text{ONOO}^-$  in live cells. Compared to the former two approaches, fluorescence-based sensing exhibits the advantages of high sensitivity and selectivity, as well as the ability to directly monitor  $\text{ONOO}^-$  concentrations and localization in real time with live cells and *in vivo*.<sup>25-27</sup> All these potential advantages make the detection method based on fluorescent probes a hot area of research for development.<sup>28-37</sup> In general, fluorescent probes respond to target analytes based on specific interactions to generate changes in fluorescence intensity.<sup>38-44</sup> However, detection methods based on emission intensities at a single wavelength are not reliable and accurate enough due to the interference from the environment and probe concentrations.<sup>45-50</sup> Ratio-metric fluorescent probes designed based on Föster resonance energy transfer (FRET) can avoid these kind of interference to a significant extent.<sup>47,51</sup> Based on non-radiative dipole-dipole interaction, the energy of a fluorophore donor in an excited state can transfer to a fluorophore acceptor in the ground state.<sup>52,53</sup> Due to the process of FRET, two fluorescent signals at different wavelengths can be measured at the same time. This method is more accurate because of the built-in correction and avoids interference caused by environmental and concentration changes.<sup>45,53,54</sup>

Carbon dots (CDs), are zero-dimensional nanomaterial with sizes typically less than 10 nm, consisting of  $\text{sp}^3$  hybridized carbon cores with partial  $\text{sp}^2$  hybridized carbon domains and shells rich with carboxyl, amino and hydroxyl groups.<sup>55-59</sup> The photoluminescence of CDs is in part dependent on  $\text{sp}^2$  and  $\text{sp}^3$  carbon defects.<sup>60-63</sup> Besides, CDs exhibit long absorption and emission wavelengths, large Stokes shift and excellent biocompatibility. In addition, due to their high fluorescence quantum yields, CDs can improve the sensitivity of the whole detection system. At the same time, their excellent water solubility and photostability can help inhibit the aggregation of fluorophores.<sup>57,64,65</sup> Compared with traditional molecular fluorophores, the optical properties of CDs make them suitable as energy donors to construct FRET-based ratiometric fluorescent probes.<sup>65,66</sup>

In our previous work, DSPE-PEG 2000 was used to encapsulate a naphthalimide-isatin peroxy nitrite sensing system to construct an ICT-based turn-on fluorescent probe DSPE-PEG/**HN-I** to detect  $\text{ONOO}^-$  with high selectivity. However, the probe exhibited relatively poor imaging capability for endogenous  $\text{ONOO}^-$  in live cells.<sup>67</sup> Consequently, inspired by the properties of CDs, we developed a FRET-based ratiometric nano probe **CD-N-I** to detect  $\text{ONOO}^-$  with high selectivity (Scheme 1). Therefore, with **CD-N-I**, CDs were used as energy donors and a naphthalimide fluorophore was used as an energy acceptor to



Scheme 1 Schematic diagram of the mechanism of peroxy nitrite detection using **CD-N-I**.

construct an effective FRET platform based on electrostatic interactions. The addition of  $\text{ONOO}^-$  can trigger the activation of the isatin receptor and switch on the FRET process. This kind of ratiometric detection is more reliable due to reduced interference by environment factors. The supramolecular assembly of probes with CDs is a particularly simple approach by which to design FRET-type sensors as well as reducing the typical aggregation-caused quenching of naphthalimide based fluorescent probes. In addition, compared to using **N-I** alone, **CD-N-I** is more sensitive towards the detection of  $\text{ONOO}^-$ . As such, **CD-N-I** could be used to image endogenous  $\text{ONOO}^-$  in APAP-induced live cells. These results confirm the potential of **CD-N-I** for the detection of  $\text{ONOO}^-$  in APAP-induced DILI.

## Results and discussion

### Preparation and characterization

In order to obtain the nano probe **CD-N-I** for the detection of  $\text{ONOO}^-$ , we independently synthesized CDs and the naphthalimide-isatin peroxy nitrite sensing system **N-I**. Citric acid and ethylenediamine were heated at 180 °C for 1 hour to synthesize CDs based on the hydrothermal method.<sup>65,68</sup> As shown by the TEM image (Fig. 1a and b), CDs were obtained as quasi-spherical structures and were well dispersed with diameters ranging from 1.3 nm to 4.5 nm. From Fig. 1c, the lattice spacing of CDs was about 0.21 nm. Based on the XPS spectrum of the CDs (Fig. S1a, ESI†), three main peaks at 532.2 eV, 399.1 eV and 284.7 eV correspond to O 1s, N 1s and C 1s respectively. From the high-resolution XPS spectrum of C 1s (Fig. S1b, ESI†), the peaks at 284.8 eV, 286.4 eV and 288.7 eV correspond to the C-C/C=C, C-O/C-N and C=O respectively. For the high-resolution XPS spectrum of O 1s (Fig. S1c, ESI†), the peaks at 532.4 eV and 532.5 eV correspond to the C=O and C-OH respectively. The high-resolution XPS spectrum of N 1s also shows two peaks at 398.2 eV and 399.4 eV corresponding to the C-N and N-H respectively (Fig. S1d, ESI†).<sup>69,70</sup> The CDs were also characterized by FT-IR infrared spectroscopy. As shown in



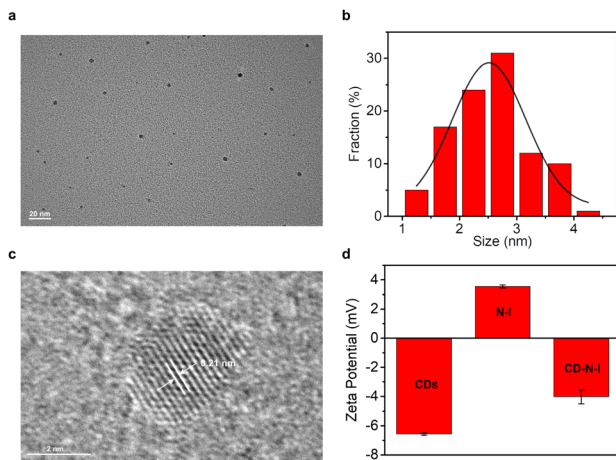


Fig. 1 (a) TEM image of CDs. (b) The diameter distribution of CDs. (c) HR-TEM image of CDs. (d) Zeta potential of CDs ( $37.2 \mu\text{g mL}^{-1}$ ), N-I ( $147 \mu\text{M}$ ) and CD-N-I ( $72.3 \mu\text{g mL}^{-1}$ ) in deionized water (containing 1% DMSO).

Fig. S2† (black line), the stretching vibration of O–H and N–H correspond to the absorption at  $3000\text{--}3500 \text{ cm}^{-1}$ . Meanwhile, the stretching vibration C=O and C–N were observed at  $1000\text{--}1750 \text{ cm}^{-1}$ . These results indicate that CDs are rich with carboxyl and amino groups.

Two absorptions at 245 nm and 350 nm in the UV-Vis spectrum of the CDs correspond to the transition of  $\pi\text{--}\pi^*$  and  $n\text{--}\pi^*$  (Fig. S3a, ESI†).<sup>65,71</sup> As expected, CDs exhibit excitation-independent emission (Fig. S3b, ESI†). When the CDs were excited by wavelengths ranging from 350 nm to 420 nm, there was no obvious red shift of the emission spectra just decreasing fluorescence intensities. To date, the photoluminescent mechanism of CDs is still not fully understood. It is possible that conjugated  $\pi$ -domains and surface states tune the photoluminescence of the CDs.<sup>72–75</sup> It has been suggested that the emission of the synthesized CDs follows Kasha Rules, which

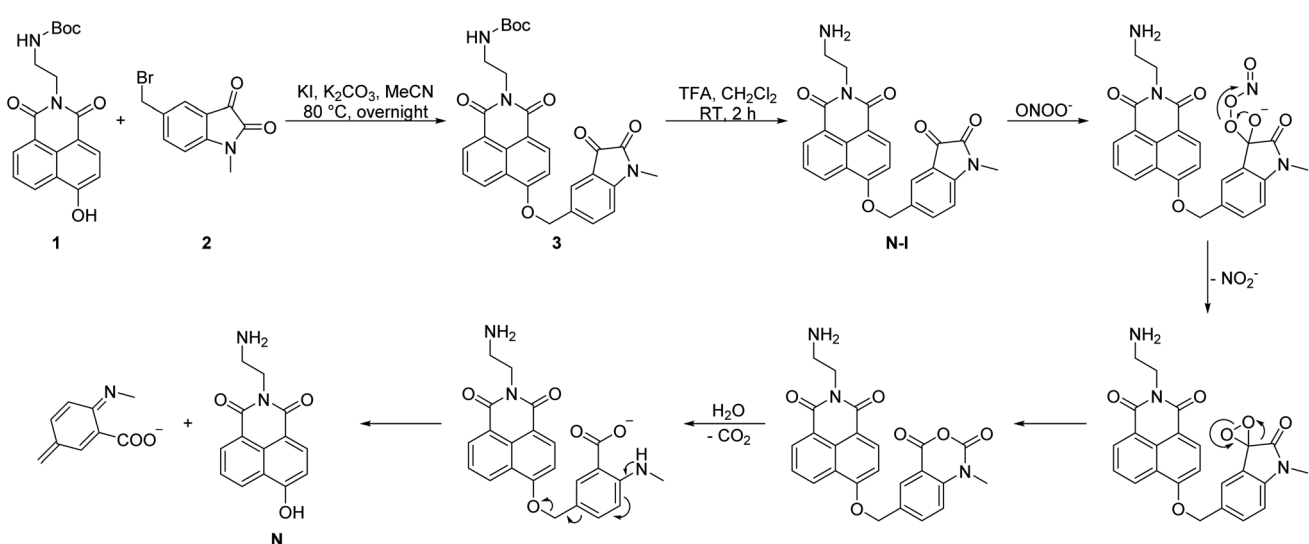
also explains their excitation-independent fluorescence behaviour.<sup>76,77</sup>

We readily obtained **N-I** (Scheme 2).<sup>26,67,78–81</sup> The naphthalimide fluorophore with Boc protection **1** and the isatin group **2** were separately synthesized (Scheme S1, ESI†). Then, the two parts were linked by a nucleophilic reaction and compound **3** was obtained in a yield of 26%. TFA was then used to deprotect the Boc group and obtain **N-I**. All the compounds obtained were fully characterized using NMR, IR and HRMS.

A solution of **CD-N-I** was prepared by mixing two stock solutions of  $2.48 \text{ mg mL}^{-1}$  CDs and  $9.78 \text{ mM}$  **N-I** in PBS buffer ( $5.5 \text{ mM}$ , pH = 7.4) with a ratio of 1:1 for 30 minutes.<sup>65,82</sup> The zeta potential was used to confirm the assembly between the CDs and **N-I** (Fig. 1d). The zeta potential value of the CDs is  $-6.56 \text{ mV}$  while the zeta potential value of **N-I** was  $3.55 \text{ mV}$ . After self-assembly, the zeta potential value of the nano probe **CD-N-I** was  $-4.02 \text{ mV}$ . This value confirms the assembly of CDs and **N-I** was based on electrostatic interactions.<sup>82–85</sup>

### Spectral properties of CD-N-I

In order to construct an efficient FRET platform between the CDs and **N-I**, the excitation wavelength of the CDs was selected according to the absorption wavelength of **N-I**. Based on UV-Vis and fluorescence spectra, when CDs were excited at 400 nm, there was a maximal overlap between the emission spectrum of the CDs and the absorption spectra of **N-I** (Fig. S4, ESI†). Therefore, 400 nm was selected as the most suitable excitation wavelength for **CD-N-I**. The fluorescence properties of **CD-N-I** were then evaluated in PBS buffer ( $5.5 \text{ mM}$ , containing 1% DMSO) at pH = 7.4 and 25 °C. As shown in the UV-Vis spectrum (Fig. 3a), after the addition of  $\text{ONOO}^-$ , a new absorption at 450 nm in addition to the original absorption at about 400 nm was observed. The fluorescence properties of **CD-N-I** were then investigated. Due to the isatin group, the ICT process of the naphthalimide fluorophore was inhibited so that the FRET



Scheme 2 The synthetic route of **N-I** and its proposed reaction mechanism with  $\text{ONOO}^-$ .



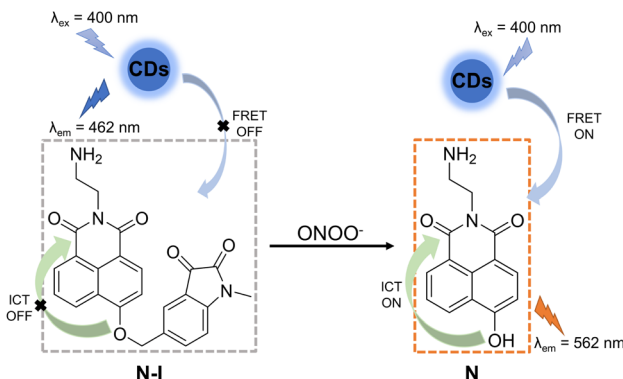


Fig. 2 The proposed mechanism of CD-N-I with  $\text{ONOO}^-$ .

process was in an off state (Fig. 2). So, there was only one emission at 462 nm when excited at 400 nm (Fig. 3b). As expected, upon the addition of  $\text{ONOO}^-$ , cleavage of the isatin group turned on the ICT process of the naphthalimide fluorophore and switched on the FRET process from the CDs to N (Fig. 2).<sup>67</sup> Due to the efficient energy transfer, a decreasing emission at 462 nm and an increasing emission at 562 nm with higher concentrations of  $\text{ONOO}^-$  was observed (Fig. 3b). For concentrations of  $\text{ONOO}^-$  ranging from 0  $\mu\text{M}$  to 40  $\mu\text{M}$ , the fluorescence intensity ratio  $I_{562}/I_{462}$  increased linearly (Fig. 3c).

The limit of detection of CD-N-I for  $\text{ONOO}^-$  detection was determined as 0.22  $\mu\text{M}$ . Significantly, compared to using N-I alone, CD-N-I is more sensitive towards  $\text{ONOO}^-$ , especially at low concentrations (Fig. S5, ESI†).

We then evaluated the pH sensitivity of CD-N-I by measuring the ratio of fluorescence intensities at  $I_{562}/I_{462}$  in solutions with different pH values ranging from 4.0 to 9.0 (Fig. 3d). The results indicated that CD-N-I exhibited low sensitivity to pH changes, which confirms that it can be used in biological systems. Based on Fig. S6† and 3d, CD-N-I displayed good pH stability which was better than that observed for just CDs or N-I. As shown in Fig. 3e, about one minute was needed to complete the reaction. This result indicated that CD-N-I can respond rapidly to  $\text{ONOO}^-$ . Results shown in Fig. S7† indicate good photostability of CD-N-I in the absence and presence of  $\text{ONOO}^-$  upon exposure to 365 nm light irradiation for 70 minutes. The thermal stability of the material was also evaluated (Fig. S8, ESI†). In the absence and presence of  $\text{ONOO}^-$ , no obvious changes in the  $I_{562}/I_{462}$  ratio of CD-N-I were observed over a temperature range from 25 °C to 45 °C, confirming its potential for use in cell imaging at 37 °C. Finally, the selectivity of CD-N-I was evaluated (Fig. 3f and S9, ESI†). Upon the addition of competing ROS and metal ions ( $\text{ROO}^\bullet$ ,  $\text{H}_2\text{O}_2$ ,  $\text{ClO}^-$ ,  $\text{O}_2^-$ ,  $\cdot\text{OH}$ ,  $^1\text{O}_2$ ,  $\text{Fe}^{2+}$ ,  $\text{Fe}^{3+}$ ,  $\text{Cu}^{2+}$ ,  $\text{Zn}^{2+}$ ,  $\text{Co}^{2+}$ ,  $\text{Mn}^{2+}$  and  $\text{Se}^{4+}$ ), minimal changes in the fluorescence

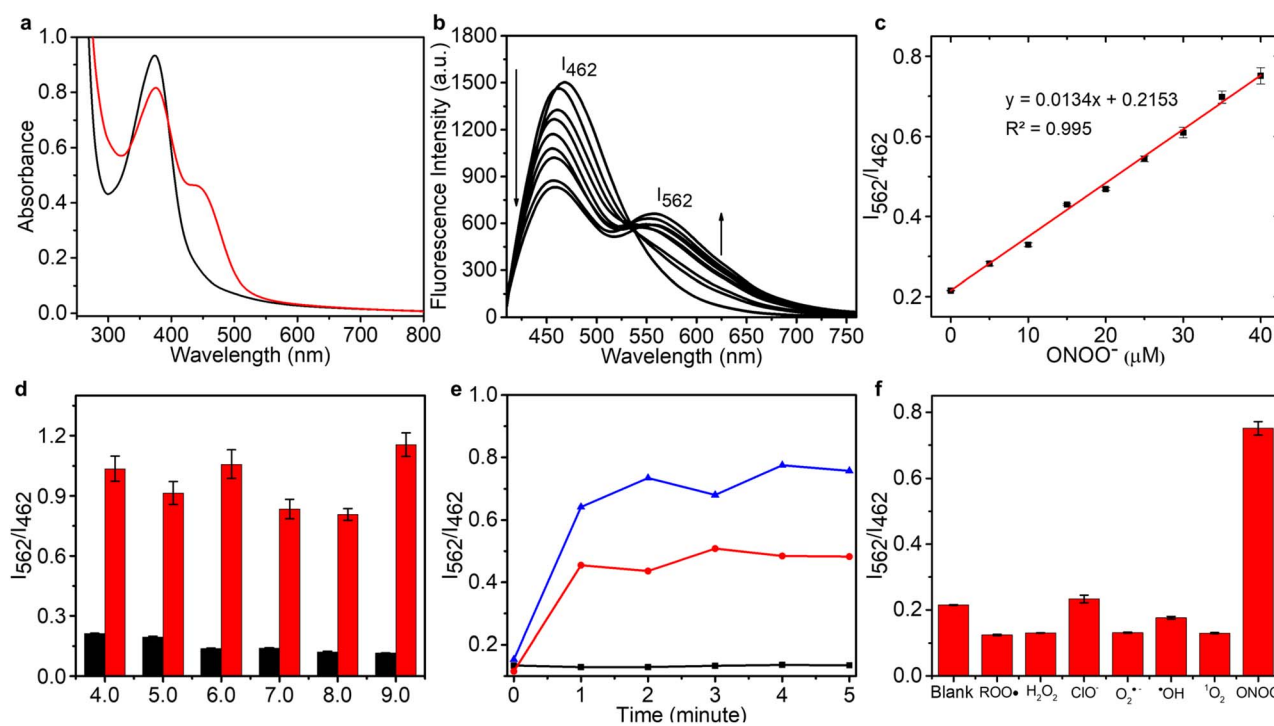


Fig. 3 (a) UV-Vis spectra of 72.3  $\mu\text{g}$  per mL CD-N-I without (black line) or with (red line) the addition of 40  $\mu\text{M}$   $\text{ONOO}^-$ . (b) Emission spectra for CD-N-I (72.3  $\mu\text{g}$   $\text{mL}^{-1}$ ) in the presence of  $\text{ONOO}^-$  (0, 5, 10, 15, 20, 25, 30, 35, 40  $\mu\text{M}$ ). (c) Linear fluorescence ratio  $I_{562}/I_{462}$  of CD-N-I towards  $\text{ONOO}^-$  (0–40  $\mu\text{M}$ ). (d) Effects pH on the fluorescence intensities of CD-N-I (72.3  $\mu\text{g}$   $\text{mL}^{-1}$ ) with (red bars) or without (black bars) the addition of  $\text{ONOO}^-$  (40  $\mu\text{M}$ ). (e) Time dependence of 72.3  $\mu\text{g}$  per mL CD-N-I with the addition of  $\text{ONOO}^-$  at concentrations of 0  $\mu\text{M}$  (black line), 20  $\mu\text{M}$  (red line) and 40  $\mu\text{M}$  (blue line). (f) Selectivity data for CD-N-I (72.3  $\mu\text{g}$   $\text{mL}^{-1}$ ) in the presence of  $\text{ONOO}^-$  (40  $\mu\text{M}$ ),  $\cdot\text{OH}$  (500  $\mu\text{M}$ ),  $\text{O}_2^-$  (500  $\mu\text{M}$ ),  $^1\text{O}_2$  (500  $\mu\text{M}$ ) after 5 minutes.  $\text{H}_2\text{O}_2$  (1 mM),  $\text{ROO}^\bullet$  (500  $\mu\text{M}$ ) and  $\text{ClO}^-$  (500  $\mu\text{M}$ ) were measured after 30 minutes. The data was obtained in PBS buffer (5.5 mM, containing 1% DMSO), pH = 7.4 at 25 °C,  $\lambda_{\text{ex}} = 400$  nm,  $\lambda_{\text{em}} = 462$  nm and 562 nm.



intensity ratio  $I_{562}/I_{462}$  were observed, which confirms the high selectivity of **CD-N-I** for  $\text{ONOO}^-$ .

### Live cell imaging

Before imaging  $\text{ONOO}^-$  in live cells, the cell viability of **CD-N-I** was assessed in live HepG2 cells using a cell counting kit-8 (CCK-8) assay. After 72.3  $\mu\text{g}$  per mL **CD-N-I** was incubated with the cells for 6 hours or 24 hours, minimal cell death was observed, which confirms the low cytotoxicity of **CD-N-I** (Fig. S10, ESI†). Then, **CD-N-I** was evaluated for imaging exogenous and endogenous  $\text{ONOO}^-$  respectively in HepG2 cells. Cells were pre-treated with 3-morpholinosydnonimine hydrochloride (SIN-1, a known  $\text{ONOO}^-$  donor) or *N*-acetylcysteine (NAC, an  $\text{ONOO}^-$  scavenger).<sup>86,87</sup> We observed that when cells were pre-treated with SIN-1, the fluorescence intensity ratio ( $I_{\text{G}}/I_{\text{B}}$ ) of the **CD-N-I** in HepG2 exhibited a significant concentration-dependent enhancement with respect to the control group (Fig. 4a and c and S11, ESI†). However, upon pre-treatment of cells with NAC, the increase in fluorescence

intensity ratio ( $I_{\text{G}}/I_{\text{B}}$ ) of **CD-N-I** that was induced by SIN-1 was attenuated (Fig. 4a and c).

Given the high expression of  $\text{ONOO}^-$  in cells induced by certain hepatotoxic drugs, we then investigated the applicability of using **CD-N-I** for the real-time monitoring of DILI. We used acetaminophen (APAP), a painkiller and antipyretic, to induce hepatocytes (HepG2 cells) a classic cell model for DILI research.<sup>88</sup> Strong blue fluorescence and weak green fluorescence were observed in APAP-free HepG2 cells (Fig. 4b and d and S12, ESI†). However, pre-treatment of cells with APAP (4 mM) for 24 h and 48 h led to a significant time-dependent increase in the fluorescence ratio (G/B) of **CD-N-I** (Fig. S12, ESI†). To confirm that the fluorescence ratio ( $I_{\text{G}}/I_{\text{B}}$ ) was triggered by the excessive production of  $\text{ONOO}^-$ , HepG2 cells were preincubated with NAC, an agent that mitigates APAP-induced hepatotoxicity. The results aligned with our expectations, as there was a marked decrease in fluorescence intensity ratio ( $I_{\text{G}}/I_{\text{B}}$ ) due to the reduced  $\text{ONOO}^-$  production (Fig. 4b and d). These findings demonstrate that **CD-N-I** can not only monitor

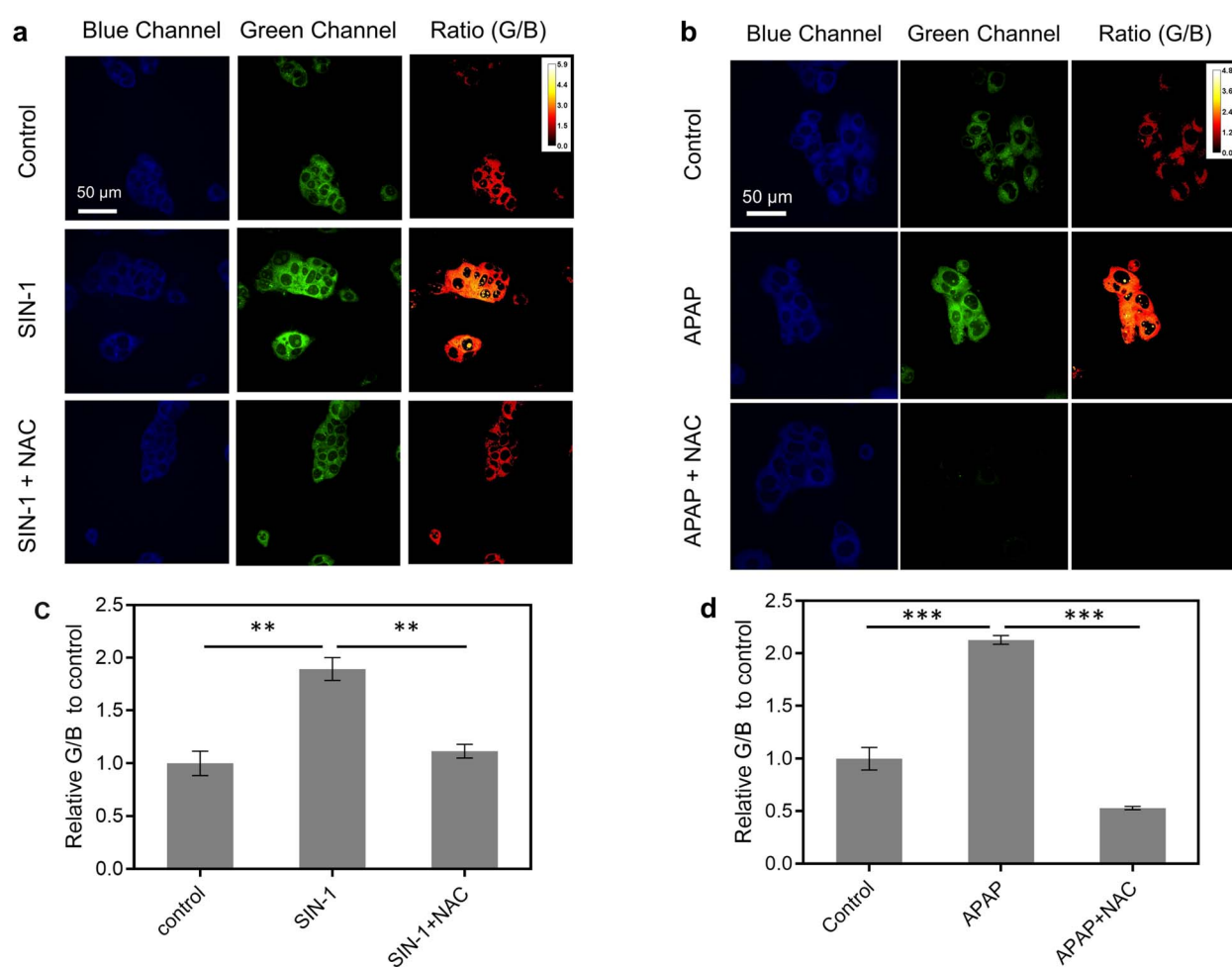


Fig. 4 (a) Fluorescence imaging and (c) fluorescence quantification of HepG2 cells treated with the **CD-N-I** (72.3  $\mu\text{g}$  mL $^{-1}$ , 2 h) in the absence and presence of SIN-1 (2 mM) and NAC (1 mM). Fluorescence data was collected using  $\lambda_{\text{ex}} = 405\text{ nm}$ ,  $\lambda_{\text{em}} = 440\text{--}500\text{ nm}$  and 540–600 nm. \*\* $P < 0.01$ . Error bars represent S. D. ( $n = 3$ ). (b) Fluorescence imaging and (d) fluorescence quantification of HepG2 cells treated with the **CD-N-I** (72.3  $\mu\text{g}$  mL $^{-1}$ , 2 h) in the absence and presence of APAP (4 mM) and NAC (1 mM). Fluorescence data was collected using  $\lambda_{\text{ex}} = 405\text{ nm}$ ,  $\lambda_{\text{em}} = 440\text{--}500\text{ nm}$  and 540–600 nm. \*\*\* $P < 0.001$ . Error bars represent S. D. ( $n = 3$ ).



and visualize the process of liver injury but could also be used to assess the efficacy of hepatoprotective drugs in hepatocytes.

## Conclusions

In brief, we have developed a self-assembled FRET-based ratio-metric nano probe **CD-N-I** formed by electrostatic interactions between CDs and a naphthalimide-isatin peroxy nitrite sensing system. On reaction with  $\text{ONOO}^-$ , the isatin is cleaved which switches on the FRET process from the CDs to the naphthalimide fluorophore. Based on the sensing performance in solution and live cells, **CD-N-I** exhibits high selectivity and excellent sensitivity towards  $\text{ONOO}^-$  over other ROS. At the same time, due to its low cytotoxicity, excellent water solubility and photostability, **CD-N-I** was successfully used to image exogenous and endogenous  $\text{ONOO}^-$  in live cells. In particular, the imaging ability of **CD-N-I** in APAP-induced cells indicates that the probe has great potential for applications in evaluating DILI.

## Data availability

The authors confirm that the data supporting the findings of this study are available within the article ESI.†

## Author contributions

Yueci Wu: conceptualization, data curation, formal analysis, investigation, methodology, validation, visualization, writing – original draft, writing – review & editing. Lu-Lu Sun: data curation, formal analysis, investigation, methodology, validation, visualization, writing – original draft. Hai-Hao Han: funding acquisition, project administration, resources, supervision, writing – original draft, writing – review & editing. Xiao-Peng He: funding acquisition, project administration, resources, supervision, writing – original draft, writing – review & editing. Weiguo Cao: funding acquisition, project administration, resources, supervision, writing – original draft, writing – review & editing. Tony D. James: conceptualization, funding acquisition, methodology, project administration, supervision, visualization, writing – original draft, writing – review & editing.

## Conflicts of interest

There are no conflicts to declare.

## Acknowledgements

Y. W. wishes to thank China Scholarship Council, the University of Bath and Shanghai University. T. D. J. wishes to thank the University of Bath and the Open Research Fund of the School of Chemistry and Chemical Engineering, Henan Normal University (2020ZD01) for support. H.-H. H. thanks the National Natural Science Foundation of China (No. 22107029, 22377135), the Fundamental Research Projects of Science & Technology Innovation and development Plan in Yantai City (2023JCYJ059), and the Shandong Laboratory Program (SYS202205). X.-P. H.

thanks the National Natural Science Foundation of China (No. 21788102, 91853201 and 9185920077).

## References

- 1 L. Y. Yuan and N. Kaplowitz, *Clin. Liver Dis.*, 2013, **17**, 48–54.
- 2 S. David and J. P. Hamilton, *US Gastroenterol. Hepatol. Rev.*, 2010, **6**, 73–80.
- 3 D. A. Smith and E. F. Schmid, *Curr. Opin. Drug Discovery Dev.*, 2006, **9**, 38–46.
- 4 T. R. Knight, A. Kurtz, M. L. Bajt, J. A. Hinson and H. Jaeschke, *Toxicol. Sci.*, 2001, **62**, 212–220.
- 5 E. Yoon, A. Babar, M. Choudhary, M. Kutner and N. Pyrsopoulos, *J. Clin. Transl. Hepatol.*, 2016, **4**, 131–142.
- 6 H. Jaeschke, *J. Pharmacol. Exp. Ther.*, 1990, **255**, 935–941.
- 7 A. Berson, S. Renault, P. Letteron, M. A. Robin, B. Fromenty, D. Fau, M. A. LeBot, C. Riche, A. M. DurandSchneider, G. Feldmann and D. Pessaire, *Gastroenterology*, 1996, **110**, 1878–1890.
- 8 J. A. Hinson, S. L. Pike, N. R. Pumford and P. R. Mayeux, *Chem. Res. Toxicol.*, 1998, **11**, 604–607.
- 9 R. Radi, G. Peluffo, M. N. Alvarez, M. Naviliat and A. Cayota, *Free Radical Biol. Med.*, 2001, **30**, 463–488.
- 10 C. Szabo, H. Ischiropoulos and R. Radi, *Nat. Rev. Drug Discovery*, 2007, **6**, 662–680.
- 11 M. P. Holt and C. Ju, *AAPS J.*, 2006, **8**, E48–E54.
- 12 G. Ferrer-Sueta, N. Campolo, M. Trujillo, S. Bartesaghi, S. Carballa, N. Romero, B. Alvarez and R. Radi, *Chem. Rev.*, 2018, **118**, 1338–1408.
- 13 R. S. Ronson, M. Nakamura and J. Vinent-Johansen, *Cardiovasc. Res.*, 1999, **44**, 47–59.
- 14 M. Sandoval, X. J. Zhang, X. P. Liu, E. E. Mannick, D. A. Clark and M. J. S. Miller, *Free Radical Biol. Med.*, 1997, **22**, 489–495.
- 15 E. L. Taylor, I. L. Megson, C. Haslett and A. G. Rossi, *Cell Death Differ.*, 2003, **10**, 418–430.
- 16 X. Chen, H. Chen, R. Deng and J. Shen, *Biomed. J.*, 2014, **37**, 120–126.
- 17 A. Vasilescu, M. Gheorghiu and S. Peteu, *Microchim. Acta*, 2017, **184**, 649–675.
- 18 F. Bedioui, D. Quinton, S. Griveau and T. Nyokong, *Phys. Chem. Chem. Phys.*, 2010, **12**, 9976–9988.
- 19 B. B. Wang, X. P. Ji, J. J. Ren, R. X. Ni and L. Wang, *Bioelectrochemistry*, 2017, **118**, 75–82.
- 20 W. C. A. Koh, J. I. Son, E. S. Choe and Y. B. Shim, *Anal. Chem.*, 2010, **82**, 10075–10082.
- 21 K. S. Jiao, S. Mandapati, P. L. Skipper, S. R. Tannenbaum and J. S. Wishnok, *Anal. Biochem.*, 2001, **293**, 43–52.
- 22 H. Ahsan, *Hum. Immunol.*, 2013, **74**, 1392–1399.
- 23 J. S. Althaus, K. R. Schmidt, S. T. Fountain, M. T. Tseng, R. T. Carroll, P. Galatsis and E. D. Hall, *Free Radical Biol. Med.*, 2000, **29**, 1085–1095.
- 24 M. Bandoorkwala, D. Thakkar and P. Sengupta, *Crit. Rev. Anal. Chem.*, 2020, **50**, 265–289.
- 25 W. L. Cui, M. H. Wang, Y. H. Yang, J. Y. Wang, X. Z. Zhu, H. T. Zhang and X. X. Ji, *Coord. Chem. Rev.*, 2023, **474**, 214848–214866.



26 S. Wang, L. Y. Chen, P. Jangili, A. Sharma, W. Li, J. T. Hou, C. Q. Qin, J. Yoon and J. S. Kim, *Coord. Chem. Rev.*, 2018, **374**, 36–54.

27 Q. Q. Ma, S. L. Xu, Z. D. Zhai, K. Wang, X. L. Liu, H. B. Xiao, S. P. Zhuo and Y. Y. Liu, *Chem.-Eur. J.*, 2022, **28**, 1–14.

28 L. Wang, M. S. Frei, A. Salim and K. Johnsson, *J. Am. Chem. Soc.*, 2019, **141**, 2770–2781.

29 X. Tian, L. C. Murfin, L. L. Wu, S. E. Lewis and T. D. James, *Chem. Sci.*, 2021, **12**, 3406–3426.

30 D. Wu, A. C. Sedgwick, T. Gunnlaugsson, E. U. Akkaya, J. Yoon and T. D. James, *Chem. Soc. Rev.*, 2017, **46**, 7105–7123.

31 Z. Q. Guo, S. Park, J. Yoon and I. Shin, *Chem. Soc. Rev.*, 2014, **43**, 16–29.

32 H. H. Han, H. Tian, Y. Zang, A. C. Sedgwick, J. Li, J. L. Sessler, X. P. He and T. D. James, *Chem. Soc. Rev.*, 2021, **50**, 9391–9429.

33 H. H. Han, H. M. Wang, P. Jangili, M. L. Li, L. L. Wu, Y. Zang, A. C. Sedgwick, J. Li, X. P. He, T. D. James and J. S. Kim, *Chem. Soc. Rev.*, 2023, **52**, 879–920.

34 W. T. Dou, H. H. Han, A. C. Sedgwick, G. B. Zhu, Y. Zang, X. R. Yang, J. Yoon, T. D. James, J. Li and X. P. He, *Sci. Bull.*, 2022, **67**, 853–878.

35 W. T. Dou, P. Qiu, Y. Y. Shi, L. Zhu, C. Guo, N. Li, Y. Zang, T. T. Liu, S. W. Zhao, Y. F. Pan, L. W. Dong, J. L. Sessler, Y. X. Tan, J. Li, H. Y. Wang, H. Tian and X. P. He, *J. Am. Chem. Soc.*, 2023, **145**, 17377–17388.

36 X. L. Hu, H. Q. Gan, Z. Y. Qin, Q. Liu, M. Li, D. J. Chen, J. L. Sessler, H. Tian and X. P. He, *J. Am. Chem. Soc.*, 2023, **145**, 8917–8926.

37 W. T. Dou, X. Wang, T. T. Liu, S. W. Zhao, J. J. Liu, Y. Yan, J. Li, C. Y. Zhang, A. C. Sedgwick, H. Tian, J. L. Sessler, D. M. Zhou and X. P. He, *Chem.*, 2022, **8**, 1750–1761.

38 L. You, D. J. Zha and E. V. Anslyn, *Chem. Rev.*, 2015, **115**, 7840–7892.

39 Y. H. Fu and N. S. Finney, *RSC Adv.*, 2018, **8**, 29051–29061.

40 H. Kobayashi, M. Ogawa, R. Alford, P. L. Choyke and Y. Urano, *Chem. Rev.*, 2010, **110**, 2620–2640.

41 M. Weber, H. H. Han, B. H. Li, M. L. Odyniec, C. E. F. Jarman, Y. Zang, S. D. Bull, A. B. Mackenzie, A. C. Sedgwick, J. Li, X. P. He and T. D. James, *Chem. Sci.*, 2020, **11**, 8567–8571.

42 H. H. Han, A. C. Sedgwick, Y. Shang, N. Li, T. T. Liu, B. H. Li, K. Q. Yu, Y. Zang, J. T. Brewster, M. L. Odyniec, M. Weber, S. D. Bull, J. Li, J. L. Sessler, T. D. James, X. P. He and H. Tian, *Chem. Sci.*, 2020, **11**, 1107–1113.

43 Z. Y. Jia, H. H. Han, A. C. Sedgwick, G. T. Williams, L. Gwynne, J. T. Brewster, S. D. Bull, A. T. A. Jenkins, X. P. He, H. Schonherr, J. L. Sessler and T. D. James, *Front. Chem.*, 2020, **8**, 389–394.

44 A. C. Sedgwick, H. H. Han, J. E. Gardiner, S. D. Bull, X. P. He and T. D. James, *Chem. Sci.*, 2018, **9**, 3672–3676.

45 X. L. Huang, J. B. Song, B. C. Yung, X. H. Huang, Y. H. Xiong and X. Y. Chen, *Chem. Soc. Rev.*, 2018, **47**, 2873–2920.

46 R. J. Gui, H. Jin, X. N. Bu, Y. X. Fu, Z. H. Wang and Q. Y. Liu, *Coord. Chem. Rev.*, 2019, **383**, 82–103.

47 M. H. Lee, J. S. Kim and J. L. Sessler, *Chem. Soc. Rev.*, 2015, **44**, 4185–4191.

48 X. Z. Chai, B. H. Li, C. Chen, W. J. Zhang, L. L. Sun, H. H. Han, Y. F. Zhang, S. S. Sun, J. M. Yang, J. J. Zhang and X. P. He, *Anal. Chem.*, 2023, **95**, 5747–5753.

49 L. L. Wu, J. H. Liu, X. Tian, R. R. Groleau, B. D. Feng, Y. G. Yang, A. C. Sedgwick, H. H. Han, Y. Wang, H. M. Wang, F. Huang, S. D. Bull, H. Zhang, C. S. Huang, Y. Zang, J. Li, X. P. He, P. Li, B. Tang, T. D. James and J. L. Sessler, *J. Am. Chem. Soc.*, 2022, **144**, 174–183.

50 X. Z. Chai, H. H. Han, A. C. Sedgwick, N. Li, Y. Zang, T. D. James, J. J. Zhang, X. L. Hu, Y. Yu, Y. Li, Y. Wang, J. Li, X. P. He and H. Tian, *J. Am. Chem. Soc.*, 2020, **142**, 18005–18013.

51 J. L. Fan, M. M. Hu, P. Zhan and X. J. Peng, *Chem. Soc. Rev.*, 2013, **42**, 29–43.

52 K. E. Sapsford, L. Berti and I. L. Medintz, *Angew. Chem., Int. Ed.*, 2006, **45**, 4562–4588.

53 H. T. Zhang, R. C. Liu, Y. Tan, W. H. Xie, H. P. Lei, H. Y. Cheung and H. Y. Sun, *ACS Appl. Mater. Interfaces*, 2015, **7**, 5438–5443.

54 S. H. Park, N. Kwon, J. H. Lee, J. Yoon and I. Shin, *Chem. Soc. Rev.*, 2020, **49**, 143–179.

55 H. Ding, S. B. Yu, J. S. Wei and H. M. Xiong, *ACS Nano*, 2016, **10**, 484–491.

56 X. Y. Xu, R. Ray, Y. L. Gu, H. J. Ploehn, L. Gearheart, K. Raker and W. A. Scrivens, *J. Am. Chem. Soc.*, 2004, **126**, 12736–12737.

57 X. C. Li, S. J. Zhao, B. L. Li, K. Yang, M. H. Lan and L. T. Zeng, *Coord. Chem. Rev.*, 2021, **431**, 1–22.

58 N. V. Tepliakov, E. V. Kundelev, P. D. Khavlyuk, Y. Xiong, M. Y. Leonov, W. R. Zhu, A. V. Baranov, A. V. Fedorov, A. L. Rogach and I. D. Rukhlenko, *ACS Nano*, 2019, **13**, 10737–10744.

59 L. C. Zhu, W. J. Kong, J. J. Ma, R. F. Zhang, C. Qin, H. Liu and S. Pan, *J. Biol. Eng.*, 2022, **16**, 1–17.

60 F. Y. Yan, Z. H. Sun, H. Zhang, X. D. Sun, Y. X. Jiang and Z. J. Bai, *Microchim. Acta*, 2019, **186**, 1–37.

61 H. Ding, X. X. Zhou, J. S. Wei, X. B. Li, B. T. Qin, X. B. Chen and H. M. Xiong, *Carbon*, 2020, **167**, 322–344.

62 L. Ai, Y. S. Yang, B. Y. Wang, J. B. Chang, Z. Y. Tang, B. Yang and S. Y. Lu, *Sci. Bull.*, 2021, **66**, 839–856.

63 R. Shen, K. Song, H. R. Liu, Y. S. Li and H. W. Liu, *ChemPhysChem*, 2012, **13**, 3549–3555.

64 S. P. Huang, W. S. Li, P. Han, X. Zhou, J. W. Cheng, H. Y. Wen and W. M. Xue, *Anal. Methods*, 2019, **11**, 2240–2258.

65 J. S. Sidhu, A. Singh, N. Garg and N. Singh, *ACS Appl. Mater. Interfaces*, 2017, **9**, 25847–25856.

66 L. Cao, X. Wang, M. J. Meziani, F. S. Lu, H. F. Wang, P. J. G. Luo, Y. Lin, B. A. Harruff, L. M. Veca, D. Murray, S. Y. Xie and Y. P. Sun, *J. Am. Chem. Soc.*, 2007, **129**, 11318–11319.

67 Y. C. Wu, H. H. Han, L. He, L. Li, Y. Zang, J. Li, X. P. He, Y. P. Ding, W. G. Cao and T. D. James, *Chem. Commun.*, 2023, **59**, 5051–5054.

68 J. Q. Wang, P. F. Zhang, C. Huang, G. Liu, K. C. F. Leung and Y. X. J. Wang, *Langmuir*, 2015, **31**, 8063–8073.

69 Z. H. Wen and X. B. Yin, *RSC Adv.*, 2016, **6**, 27829–27835.



70 H. Z. Liu, X. Zhao, F. Wang, Y. P. Wang, L. Guo, J. J. Mei, C. C. Tian, X. T. Yang and D. X. Zhao, *Nanoscale Res. Lett.*, 2017, **12**, 1–7.

71 S. N. Baker and G. A. Baker, *Angew. Chem., Int. Ed.*, 2010, **49**, 6726–6744.

72 X. H. Zhu, X. Xiao, X. X. Zuo, Y. Liang and J. M. Nan, *Part. Part. Syst. Charact.*, 2014, **31**, 801–809.

73 C. Shen, Y. P. Sun, J. Wang and Y. Lu, *Nanoscale*, 2014, **6**, 9139–9147.

74 S. J. Wang, Z. G. Chen, I. Cole and Q. Li, *Carbon*, 2015, **82**, 304–313.

75 P. Yu, X. M. Wen, Y. R. Toh and J. Tang, *J. Phys. Chem. C*, 2012, **116**, 25552–25557.

76 Y. Q. Zhang, Y. S. Hu, J. Lin, Y. Fan, Y. T. Li, Y. Lv and X. Y. Liu, *ACS Appl. Mater. Interfaces*, 2016, **8**, 25454–25460.

77 Y. Q. Zhao, X. G. Liu, Y. Z. Yang, L. T. Kang, Z. Yang, W. F. Liu and L. Chen, *Fullerenes, Nanotubes Carbon Nanostruct.*, 2015, **23**, 922–929.

78 J. H. Xiong, W. W. Wang, C. X. Wang, C. Zhong, R. Q. Ruan, Z. Q. Mao and Z. H. Liu, *ACS Sens.*, 2020, **5**, 3237–3245.

79 P. R. Su, Z. W. Zhu, Y. H. Tian, L. J. Liang, W. Y. Wu, J. Cao, B. Cheng, W. S. Liu and Y. Tang, *Talanta*, 2020, **218**, 121127–121134.

80 E. E. Rudebeck, R. P. Cox, T. D. M. Bell, R. Acharya, Z. K. Feng, N. Gueven, T. D. Ashton and F. M. Pfeffer, *Chem. Commun.*, 2020, **56**, 6866–6869.

81 R. F. Ohana, T. A. Kirkland, C. C. Woodroffe, S. Levin, H. T. Uyeda, P. Otto, R. Hurst, M. B. Robers, K. Zimmerman, L. P. Encell and K. V. Wood, *ACS Chem. Biol.*, 2015, **10**, 2316–2324.

82 Y. Y. He, Z. X. Li, Q. Y. Jia, B. J. Shi, H. Y. Zhang, L. H. Wei and M. M. Yu, *Chin. Chem. Lett.*, 2017, **28**, 1969–1974.

83 M. Kaszuba, J. Corbett, F. M. Watson and A. Jones, *Philos. Trans. R. Soc., A*, 2010, **368**, 4439–4451.

84 S. Honary and F. Zahir, *Trop. J. Pharm. Res.*, 2013, **12**, 255–264.

85 H. Qu, H. Ma, W. Zhou and C. J. O'Connor, *Inorg. Chim. Acta*, 2012, **389**, 60–65.

86 K. Shirai, T. Okada, K. Konishi, H. Murata, S. Akashi, F. Sugawara, N. Watanabe and T. Arai, *Oxid. Med. Cell. Longevity*, 2012, **2012**, 326731–326745.

87 R. Foresti, P. Sarathchandra, J. E. Clark, C. J. Green and R. Motterlini, *Biochem. J.*, 1999, **339**, 729–736.

88 M. Z. Yan, Y. Z. Huo, S. T. Yin and H. B. Hu, *Redox Biol.*, 2018, **17**, 274–283.

